Oxidation behaviour of a developmental nickel-based alloy and the role of minor elements

Taylor, Mary; Ding, Rengen; Mignanelli, Paul M.; Hardy, Mark

DOI:
10.1016/j.corsci.2021.110002

Document Version
Peer reviewed version

Citation for published version (Harvard):
Taylor, M, Ding, R, Mignanelli, PM & Hardy, M 2022, 'Oxidation behaviour of a developmental nickel-based alloy and the role of minor elements', *Corrosion Science*, vol. 196, 110002.
https://doi.org/10.1016/j.corsci.2021.110002

OXIDATION BEHAVIOUR OF A DEVELOPMENTAL NICKEL-BASED ALLOY AND THE ROLE OF MINOR ELEMENTS

Authors:

Mary Taylor[a*], Rengen Ding[b], Paul Mignanelli[c] and Mark Hardy[c]

[a] University of Birmingham, B15 2TT, UK

[b] formerly University of Birmingham, UK, now Centre of Excellence for Advanced Materials, Dongguan, China.

[c] Rolls-Royce plc, Derby, DE24 8BJ, UK

* Corresponding author, School of Metallurgy and Materials, University of Birmingham, Edgbaston, Birmingham B15 2TT.

Keywords

Oxidation, nickel-based alloy, minor elements

ACKNOWLEDGEMENTS

This work was supported by the Rolls-Royce/EPSRC Strategic Partnership under EP/H022309/1. The services at the Centre of Electron Microscopy at the University of Birmingham and the help provided by Mrs Theresa Morris are gratefully acknowledged.

ABSTRACT

The oxidation kinetics of a chromia forming development nickel-based superalloy over the temperature range of 700 to 850 °C under isothermal and 100 hour thermal cycles are presented. The kinetics compare favourably with similar alloys and this is attributed to the formation of (Ti,Nb,Ta)(N,C,B) precipitates found throughout the alloy. Between 840 and 850 °C an ~~significant~~ increase in the oxidation kinetics was observed; attributed to the dissolution of the precipitates, ~~phases~~ releasing titanium, tantalum and niobium into the alloy matrix. The results are discussed in terms of potential effect of the presence of (N,C,B) phases and stability on the oxidation kinetics. ~~This demonstrated clearly the role of these elements on the oxidation kinetics of the alloy.~~

1. Introduction

Nickel-based superalloys are designed to operate in highly stressed conditions under oxidising environments at high temperatures. Optimum materials properties are achieved both compositionally and by the use of heat treatments [1, 2] and the oxidation protection is afforded in these alloys by the formation of a surface oxide. The surface oxide formed reflects the composition of the alloy and operating conditions, as demonstrated for ternary (Ni, Cr, Al) alloys at temperatures above 1000°C by Giggins et. al. [3]. That work clearly showed that a minimum critical concentration of the element forming the surface oxide was necessary for a complete coverage of the surface to be achieved. For Cr_2O_3 forming Ni-based alloys a compositional range of chromium 8 to 17 wt.% has been reported [4-6]. The critical concentration of chromium necessary was found to decrease as the aluminium content of the alloys increased with some effect of temperature on the actual value. At lower temperatures, i.e. 650°C, it is reported that a minimum concentration of chromium of 16 wt.% is necessary to form a surface layer of Cr_2O_3 [4] although it has been demonstrated that the oxide formed on alloys with chromium values as low as 13 wt.% (at 800°C) [5, 6], possibly due to the influence of the other alloying additions.

One application for these high strength alloys is the rotor component within aero- or land-based gas turbines and many studies have been performed on the oxidation behaviour of this group of alloys [4-19]. An Arrhenius plot of the parabolic rate constants obtained from many of these papers, against the inverse of the temperature, has been published in ref. 18, demonstrating that the oxidation kinetics for Cr_2O_3 forming alloys can vary by an order of magnitude and in all cases were higher than the kinetics for pure Cr_2O_3 formation [20-23]. Factors that can result in the variability in the kinetics have been reported as: oxidation of other elements present in the alloy e.g. aluminium and titanium [3-5, 9]; surface finish [19]; spallation of the surface oxide, either partially or completely [4]; doping of the Cr_2O_3 which increases vacancy concentration thus enhancing diffusion rates through the oxide [5, 18, 24-27]. Multiple elements are added to this type of superalloy and the partitioning of each element to the phases present has been demonstrated in ref 28. Some of the alloying elements, added to stabilise beneficial phases, can be affected by exposure to operational temperatures and, in turn may influence the oxidation behaviour of the alloy [19, 29, 30]. One such element is niobium, which is a strong carbide former and γ' stabiliser [1, 2]. When the Gibbs free energy of formation of the oxide of niobium, Nb_2O_5, is plotted in the form of an Ellingham Diagram [32], it is shown that, from the pure metal, the stability of Nb_2O_5 is comparable to Cr_2O_3 formation

from chromium. It has also been found that, where high enough concentrations of niobium are present in the nickel-based alloys, the phase Ni_3Nb is formed [33-37]. The process whereby this occurs is described in detail in refs 36 and 37. Many such examples exist of the synergistic effects occurring on exposure of complex alloys to high temperatures in oxidising environments [29-31].

In this paper, the oxidation kinetics of a new alloy designed for aero-engine rotor applications, are presented. The composition of the alloy [38-40] contains multiple elements to achieve the required microstructure and mechanical properties for this critical component. Minor alloying additions in this alloy include, aluminium, titanium, tantalum, niobium and zirconium. The oxidation kinetics, based on mass change measurements, presented here show an improvement compared to alloys with comparable compositions. Detailed examination of the alloy has been performed and the results are explained in terms of the phases formed of the minor elements within ~~in~~ the bulk material.

2. Experimental procedure

The composition of the alloy investigated here is given in Table 1 [38-40]. As can be seen this is highly alloyed material, containing a relatively low concentration of chromium for this alloy type; added to stabilise the γ matrix and also provide oxidation protection by the formation of a surface layer of Cr_2O_3 under operational conditions. Some of the minor elemental additions, e.g. titanium, tantalum, aluminium and niobium, included to stabilise the γ′ phase, also form oxides under operational conditions.

Samples of the alloy were provided by Rolls-Royce, plc, sectioned using Electro-Discharge Machining, EDM, to dimensions of approximately 20 × 10 × 3 mm^3. All surfaces of these samples were ground on SiC paper from 400 to 1200 grit using water as a lubricant, to remove the residual stresses produced during sectioning. The corners and edges were chamfered to remove these stress concentrators. This was followed by polishing with 6 µm diamond suspension, again, using water as a lubricant. Samples were cleaned thoroughly including a final ultra-sonic clean in ethanol. The dimensions and mass of each sample were recorded prior to oxidation exposure and the specific mass per surface area (m/SA / $mg.cm^{-2}$) was calculated. In addition, one batch of samples had been shot-peened using the following conditions: 7A intensity, 110H shot and 200% coverage. These samples were measured, cleaned and weighed as above.

Isothermal oxidation testing at atmospheric pressure in air was conducted on the polished and shot-peened samples at temperatures of 700, 750, 800 and 850°C for times up to 2500 hours. Samples were placed in to alumina boats and inserted into the furnaces at temperature. An additional set of 150 hour isothermal exposures were performed at 800, 810, 820, 830, 840 and 850°C. At the end of the test periods the samples were removed from the furnaces, cooled to room temperature and reweighed. The samples were observed during the cooling stage for signs of spallation; no significant spallation was noted.

To generate more data for a statistical analysis of the oxidation behaviour of the alloy, 100 hour thermal cycles were performed on batches of 7 samples, again under atmospheric pressure in air. Samples were placed in to alumina boats and inserted into furnaces set to the test

temperatures of 700, 750 or 800°C. At the end of each 100 hour exposure the samples were removed from the furnaces, cooled to room temperature, re-weighed and stored in a desiccator ready for re-inserting into the furnaces for the next 100 hour cycle. This process was repeated for up to a total of 2000 hours. Again, the samples were observed during the cooling stages and no significant spallation of the surface oxide was observed in any of the samples.

Metallographic cross-sections were prepared by mounting selected samples in low viscosity resin under vacuum and grinding through by 1 to 2 mm on 240 grit SiC paper. This was followed by grinding on SiC papers from 400 to 1200 grit, with water as a lubricant. The cross-sections were polished using 6 µm followed by 1 µm diamond in a water-based lubricant and finished with a water-based sol. The samples were examined using Scanning Electron Microscopy, SEM, including in Back-Scattered Electron mode, BSE, and Energy Dispersive Spectroscopy, EDS. For higher resolution detail of the microstructure of the alloy, Transmission Electron Microscopy (Talos), TEM, foils were extracted using Focused Ion Beam milling, FIB, from a polished and a shot-peened sample each exposed at 800°C. An additional foil was extracted from a sample of the alloy in the as-received condition and examined under transmission mode using the 7000F JEOL SEM.

3. Results

The mass change data, obtained under isothermal conditions, for the polished and shot-peened samples, Figs. 1 (a) and (b), respectively, showed great similarity between the two surface variants at the three lower temperatures tested (700-800°C). This also showed the, as expected, temperature dependence of the oxidation behaviour for the alloy. At 850°C the mass change for both surface variants showed some similarity in that the kinetics diverged from that observed at the lower temperatures, i.e. the increase in kinetics was greater than expected based on the lower temperature data. Greater sample-to-sample variation was also observed in both surface variants at this temperature, for example, for the polished variant of the alloy, in Fig 1 (a), the sample exposed for 2500 hours demonstrated a lower mass increase than the sample exposed for 1000 hours despite there being no observable spallation occurring.

The data from the thermal cycling testing, Fig. 2, showed good agreement with the isothermal data at the same temperatures. This can be attributed to the lack of spallation occurring during testing, and thus the integrity of the surface oxide was maintained throughout. The plots also show the range of values obtained at each temperature demonstrating the variability in the oxidation behaviour of this alloy and also the temperature dependence of the oxidation process. The means +/- 1 st.dev. of these data sets were determined for further analysis.

The means of the thermal cycling specific mass change data were fitted to the standard kinetics equation:-

$$\left(\frac{\Delta m}{SA}\right)^{n} = k_n t + C \qquad (1)$$

where $\frac{\Delta m}{SA}$ is the change in mass normalised to the surface area, in mg.cm^{-2}, n is the exponent, k_n is the rate constant in (mg.cm^{-2})^{n}.s^{-1}, t is time in seconds and C is a constant, which under the experimental conditions used here can be taken as zero.

The gradients of the log vs log plots of the means of the thermal cycling data were produced to determine the exponent, n, in Eq 1, at each temperature, with the values given in Table 2. It was found that the data correlated well to parabolic behaviour at 700ºC, i.e., a value of $n = 2.06$ is very close to 2, and increasingly departed from this with increasing temperature. The rate constants for these data, k_n, were determined from the gradients of the plots of Eq. 1, as shown in Fig. 3 (a), with the values obtained presented in Table 2. As the values of n were close to 2, and to enable comparison of the oxidation behaviour determined here to other alloy systems, the data were also fitted to parabolic rate kinetics, i.e. plots with n taken as 2, Fig. 3(b), the values determined for k_p, are given in Table 2. This demonstrated that the data fitted well to parabolic kinetics, especially at the lower temperatures, and that the fit was better when using the n values determined from the data sets, as would be expected.

As fewer samples were tested under isothermal conditions parabolic behaviour was assumed in that analysis. The k_p values were calculated for both surface variants of the alloy and are presented in Table 3. Good agreement was found between the two surface variants at 700, 750 and 800 ºC. In addition, the agreement between the data obtained from the isothermal exposures and the thermal cycling testing at these temperatures was also good, Tables 2 and 3. At 850 ºC, Table 3, the difference in the k_p values obtained from the two variants of the alloy reflected the variability in the data found at this temperature, Fig. 1. To assess the large increase in oxidation kinetics occurring between 800 and 850 ºC a series of 150 hour isothermal exposures were performed. The parabolic rate constants, calculated from these individual measurements, are presented in Table 4. This showed a general systematic increase in kinetics over this temperature range with some sample-to-sample variation, e.g. the 820 ºC result was similar to that obtained at 800 ºC.

Cross-sectional examination of samples was performed to determine the oxide formed and to study the changes occurring in the sub-surface region of the alloy. Examples of the findings are given for a polished sample exposed for 2000 hours at 800ºC and a shot-peened sample exposed for 1025 hours at 800 ºC along with compositional profiles for selected elements, Figs. 4 and 5, respectively. Within the bulk of the alloy, away from the surface regions, light contrast precipitates consisting of some of the heavier elements present in the alloy were identified. In the shot-peened variant a smaller light contrast precipitate was observed forming in the sub-surface region of the samples, EDS analysis ~~using SEM~~ demonstrated these precipitates to be richer in molybdenum than the surrounding matrix phase. ~~, Fig. 5~~. Only the larger precipitates were present in the polished samples, Fig 4. EDS analysis showed that the surface oxide formed on both variants of the alloy was rich in chromium, assumed to be Cr_2O_3. Internal oxidation, leading to the formation of Al_2O_3 was also observed, shown as the dark contrast phase in the sub-surface region of the alloy. Also formed sub-surface and extending beneath the Al_2O_3 penetration depth, were sub-micrometre sized, dark contrast precipitates. EDS analysis of these showed higher concentrations of titanium compared to adjacent regions devoid of the phase. ~~along with nitrogen, suggesting TiN formation~~.

EDS profiles, shown in Figs. 4 and 5 revealed the compositional variations in the alloy extending from the surface into the bulk. This showed that, in both the polished and shot-peened variants, depletion of chromium and aluminium occurred to similar depths. However, no significant changes in the concentrations of the minor elements were detected, Figs 4(b) and 5(b). This was particularly relevant for titanium, where significant depletion had been observed in other equivalent alloys [9, 18, 19]. The concentration of titanium in the sub-surface region

was approximately 3.5 and 3.8 at.% in the two samples shown in Figs 4 and 5, which is similar to the concentration of this element in the bulk alloy, Table 1. Similarly for tantalum and niobium, although an increase in tantalum at the oxide alloy interface in the polished sample was observed at the site shown in Fig. 4.

To study the sub-surface region in more detail TEM foils were extracted from a number of locations from a polished and a shot-peened variant of the alloy, both exposed at 800 ºC for 2000 and 1025 hours, respectively. Fig. 6 shows montages of TEM images taken from these samples showing the changes occurring at the surface of the alloy due to the oxidation processes, also shown is the effect of surface condition prior to oxidation testing, polished and shot-peened (a) and (b), respectively. Internal oxides of aluminium were identified within an oxidation affected region extending from the surface into the bulk of the alloy; this region was identifiable by the change in contrast and texture compared to the unaffected bulk alloy. This difference emphasised the interface between the oxidation degraded region and the unaffected alloy. The interface in the polished variant was planar whereas in the shot-peened condition an undulating interface was present, the latter was due to recrystallisation of grains occurring in this variant due to the stresses induced during the shot-peening process, as described previously for a similar alloy [5]. It was also noted that a network of dislocations were present in the bulk alloy in both variants, i.e. polished and shot-peened. Also included in Fig. 6, indicated as boxes, are the sites presented in Figs. 7 and 8, shot-peened and polished, respectively, giving greater detail of the compositions and phases present.

Precipitates with cubic or needle-shaped morphologies were present in both variants, distributed through the alloy. Details of the morphologies and the compositions of these precipitates are presented in Fig. 7, taken from the shot-peened variant within the alloy away from the oxidation degradation region of the sample, from the site indicated in Fig. 6 (b). The results were observed to be the same in both alloy variants. The maps show the elemental distribution within the phases comprising the matrix enabling the identification of the γ′ phase and the γ matrix; most easily identified from the aluminium, chromium and cobalt maps.

Two categories of precipitates were seen throughout the bulk of the alloy. These were distinguishable by morphology differences. One was cubic in structure and consisted of a number of elements, see maps of ~~the nitrogen~~, niobium, tantalum and titanium and also the light elements of nitrogen, boron and carbon ~~maps~~ in Fig. 7. The other precipitate had a high aspect ratio and appeared to consist of nitrides of only titanium and niobium and were aligned along pile-ups of dislocations within the matrix. Examination of the elemental distribution connected with the cubic precipitates showed an interesting sequence with a centre composed of zirconium oxide. Surrounding this core was a niobium / tantalum rich layer and this, in turn, was encased in a titanium / niobium. Both sets of precipitates were seen in both the polished and shot-peened samples. EDS maps of boron and carbon show enhanced concentrations of these elements at these sites, the boron appears to only be present in the cubic precipitates whereas the carbon appears to contribute to both. This leads to the assumption that the cubic precipitates are complexes of (Ti,Nb,Ta)(N,C,B), where the presence of ZrO_2 acts as a nucleation site for the cubic structures.

Selected EDS maps are presented in Fig. 8 to demonstrate the changes to the morphology of the precipitates within the oxidation affected region of the samples ~~Within the oxidation affected outer region of the samples modifications to the microstructure had occurred~~, shown

here for the polished sample~~, Fig. 8~~. Dissolution of the γ′ phase had occurred, evident in the aluminium and titanium maps. Also, note the location of the sub-surface formation of Al_2O_3 using the aluminium and oxygen maps. Also shown is the effect of the oxidation process on the morphology of the cubic precipitates ~~nitrides~~. Comparison can be made between an unaffected nitride within the bulk alloy, in the top right-hand side of the image in Fig. 8, and those within the oxidation affected zone. The maps show that these precipitates have grown towards the surface of the sample, possibility related to the crystallographic orientation of the alloy grain. This comparison demonstrates the changes occurring in the degradation zone were due to the oxidation processes and diffusion of elements through the region to the outer surface and were not just an effect of temperature. It can be envisaged that the diffusion of elements from the dissolving γ′ precipitates react with nitrogen diffusing into the alloy nucleating on the surface of the existing phase and leading to the development of the distinctive morphology observed. The effect of the growth of the ~~nitrides~~ precipitates was to retain those metallic elements within the alloy and prevent emergence at the surface and subsequent oxidation or doping of the growing Cr_2O_3 layer.

To more fully understand the origins and development of these precipitates a foil was extracted from the as-received alloy and examined under transmission mode using the 7000F Joel, Fig. 9. This shows the presence of titanium, niobium and tantalum precipitates associated with carbon; no nitrogen or boron was identified at these locations in this sample.

4. Discussion

To assess the oxidation behaviour of the development alloy and draw comparisons to other alloys, the mass change data was plotted according to the Arrhenius relationship:

$$k_p = A.exp\left(\frac{-Q}{RT}\right) \qquad (2)$$

where k_p is the parabolic rate constant, A is the pre-exponential constant, Q is the Activation Energy for the total oxidation process for this alloy in J.mol^{-1}, R is the gas constant in J.mol^{-1} and T is temperature in Kelvin.

A plot of the $ln(k_p)$ vs $1/T$ was produced using all the parabolic rate constants determined in this ~~project~~ work, ~~(dots or crosses in~~ Fig. ~~9~~ 10). The range of data obtained from the literature for several relevant alloys [5-19] is shown as the hashed/shaded area, with the lower boundary formed by the kinetics for pure Cr_2O_3 formation on chromium or high chromium stainless steels [20-23]. The higher oxide growth kinetics obtained for this alloy reflect the contribution to the total mass gain from the oxidation of other elements present in the alloy, e.g. aluminium, titanium and tantalum, and also the interaction of various elements on the growth kinetics of Cr_2O_3, as outlined earlier. It can be seen that this alloy lies towards the lower bound of the data range for the Cr_2O_3 formation over the temperature range of 700 to 840 ºC inclusive, with a step change in the oxidation behaviour from 840 to 850 ºC where the kinetics transfer to the upper boundary of the data is shown. The gradient of the data from 700 to 840 ºC inclusive gave a value of Q for the oxidation process for this alloy of 269 kJ.mol^{-1} producing the following algorithm:-

$$k_p = 612100.exp\left(\frac{-269000}{8.314T}\right) \qquad (3)$$

Microstructural examination of the alloy in the as-received condition revealed the presence of clusters of titanium, niobium and tantalum carbides. At this point in the thermal history of the sample no nitrogen or boron was found associated with these phases. After thermal exposure and using high resolution TEM with EDS the microstructure, away from the oxidation affected region of the alloy, showed the formation of two classifications of precipitates. Fig 7. One classification of complexes contained cores of ZrO_2 potentially acting as nucleation sites and had a cubic morphology with composition (Ti,Nb,Ta)(C,N,B), the other had a high aspect ratio and was aligned to the dislocation network within the alloy and consisted of Ti, Nb and N.

The combination of phases observed in this study has been widely reported to form in other alloy systems [41-43], where it has been shown conclusively that the complexes are composed of nitrides, carbides and borides. ~~EDS maps obtained from TEM foils, Fig. 7, show the evidence of carbon and boron in the complexes present in this alloy.~~ The compositional layering of the cubic structures has been described in the literature [41, 42], nucleating on oxide particles with the size and compositions of the precipitates determined by the depletion rate and concentration of the forming elements from the surrounding matrix. ~~in terms of the localised depletion of each element during the formation process, i.e., the initial formation of the Nb (C, N ,B) phase, , depleted the local region of niobium. Once below a critical concentration of niobium the Ti (C, N, B) phase formed, nucleating on the previous phase. The growth of this layer was, again, limited by the local concentration of titanium which was depleted as the phase grew.~~ In this study clusters of carbides were found in the alloy, formed during processing, Fig. 9. It is possible that these were compositionally modified during the thermal exposure to the phases shown in Fig. 7. The diffusion of boron, for instance, through nickel-base alloys has been described in ref 31, resulting the formation of a number of additional phases. Evidence from the oxidation affected region of the samples clearly shows that these precipitates continue to grow. Further work in ongoing to more fully understand the formation and evolution of these compositional complex precipitates, including the high aspect ratio precipitates.

It is clear from this study that ZrO_2 particles act as nucleation sites for the complexes. Thus, the distribution of the phases was influenced by the ZrO_2 particle distribution in the alloy and the size and compositional make-up of the complexes was governed by the local concentration and thermodynamic stability of the various elements present. The distribution of the ZrO_2 particles is due to the powder metallurgy route of production. Zirconium in the powder particles readily oxidises during the production process, resulting in nanometre sized stable oxides finely distributed throughout the material. It is clear that the presence of the ZrO_2 particles acted as nucleation sites for the cubic shaped complexes and that the faster diffusion paths at the dislocation pile-ups influences the growth of the high aspect ratio complexes.

The heavier elements comprising the complexes were added to the alloy to stabilise the γ' phase. The effect of the formation of the complexes would be to tie-up these elements within the alloy in more thermodynamically stable phases, thus reducing the concentration in the γ / γ' matrix. The EDS maps, taken from sites at various locations within the alloys, revealed that the required γ / γ' structure had been achieved. In the region of the alloy affected by the oxidation processes dissolution of the γ' phase was evident as well as growth of the (Ti,Nb,Ta)(N,C,B) complexes. The change in morphology of both precipitates suggested a

crystallographic orientation to the dominant growth directions. The effect was again to retain elements usually found as oxides, such as titanium, within the alloy thus explaining the compositional profiles as shown in Figs. 4 and 5, where no apparent depletion of titanium had occurred. The impact would be to prevent the additional contribution to the oxidation mass change caused by the oxidation of these elements and also to reduce any doping effect on the growth rate of Cr_2O_3.

Investigations into the stability of the (Ti,NbTa)(N,C,B) complexes in steels has shown that these are unstable at temperatures of 850 ºC and higher [42]. In this study a clear step change in the oxidation behaviour of the alloy was observed between 840 and 850 ºC, Fig 10. It is proposed here that, above 840 ºC the complexes dissolve and the elements are released into the matrix. The step change in the oxidation kinetics is a clear indication of the impact of titanium, niobium and / or tantalum on the oxidation processes in these highly alloyed materials. As the elements are present in low concentrations the significant increase in kinetics must also indicate the impact of these elements on the growth rate of Cr_2O_3, i.e. by doping. There is also a suggestion in this work that there is a time dependence to the dissolution of the phases at 850 ºC as shown by comparing the k_p from the 150 hour exposed sample to the values obtained from the longer term exposures, Tables 4 and 3, respectively. Further work is needed to investigate the development of the minor element phases with increasing time and the dissolution process in more detail.

The work presented here demonstrates the impact of minor elemental additions on the oxidation behaviour of alloys. Also demonstrated in this study was the fact that no significant difference was found between the polished, and thus stress-free, and the shot-peened surface. It should be noted that the alloy in the polished condition did contain considerable dislocation networks which is under further investigation. The comparison between the polished and shot-peened variants further emphasises the significant impact minor elements can have on the oxidation processes occurring in these highly alloyed materials.

Conclusion

This paper presents an investigation into the oxidation kinetics of a development nickel-based superalloy. Testing at atmospheric conditions in laboratory air was performed over the temperature range of 700 to 850 ºC under isothermal and 100 hour thermal cycles for times up to 2000 hours. Two surface conditions were investigated; a complete study was made of the alloy in the polished stress-free state, with a limited study made under isothermal oxidation conditions of the alloy with a shot-peened surface finish.

The results showed improved oxidation kinetics compared to comparable alloys up to 840 ºC with no significant difference in the oxidation behaviour between the polished and shot-peened surfaces. The improvement has been attributed to the formation of two categories of (Ti,Nb,Ta)(N,C,B) complexes which ~~where~~ were found distributed throughout the alloy. The formation of the complexes effectively reduced the concentration of titanium, niobium and tantalum elements in the matrix of the alloy. Significantly, in the oxidation affected zone beneath the surface oxide, growth of the complexes was observed. The effect was to prevent diffusion to the surface of these elements thus preventing the formation of the oxides and reducing any doping effect on the surface Cr_2O_3 oxide. A step change in oxidation behaviour was noted between 840 and 850 ºC where dissolution of the phases is reported to occur in the literature, thereby releasing the elements into the matrix.

Data Availability

All necessary data is included within this paper.

References

[1] C.T. Sims, N.S. Stoloff and W.C. Hagel, eds. Superalloys II: High Temperature Materials for Aerospace and Industrial Power (New York: John Wiley and Sons, 1987).

[2] I. Dempster, R. Wallis, Heat treatment metallurgy of nickel-base alloys, in ASM Handbook, Volume 4E, Heat-treating of Non-ferrous alloys G.E. Totten, D.S. MacKenzie, editors (2016) ASM International®

[3] C.S. Giggins, F.S. Pettit, Oxidation of Ni-Cr-Al alloys between 1000° and 1200°C, J. Electrochem. Soc. 118 (1971) 1782-1790. doi: 10.1149/1.2407837

[4] B. Gleeson, M.A. Harper, Effects of minor alloying additions on oxidation behaviour of chromia-forming alloys, in: M. Schütze, W.J. Quadakkers, J.R.Nicholls (Eds.), Lifetime Modelling of High Temperature Corrosion Processes:(EFC 34), Maney Publishing, London, (2001) 167–177.

[5] S. Cruchley, H. Evans, M. Taylor, An overview of the oxidation of Ni-based superalloys for turbine disc applications: surface condition, applied load and mechanical performance, Materials at High Temperatures, 33 (2016) 465-475.

[6] L. Zheng, M. Zhang, J. Dong, Oxidation behaviour and mechanism of powder metallurgy Rene 95 nickel-based superalloy between 800 and 1000°C, Appl. Surf. Sci. 256 (2010) 7510-7515

[7] J. Chen, P. Rogers, J.A. Little, Oxidation behaviour of several chromia-forming commercial nickel-base superalloys, Oxid. Met. 47 (1997) 381–410.

[8] A. Encinas-Oropesa, N.J. Simms, J.R. Nicholls, G.L. Drew, J. Leggett, M.C. Hardy, Evaluation of oxidation related damage caused to a gas turbine disc alloy between 700 and 800°C, Mater. High Temp. 26 (2009) 241–249.

[9] M.P. Taylor, H.E. Evans, S. Stekovic, M.C. Hardy, The oxidation characteristics of the Ni-based superalloy, RR1000, at temperatures 700–900°C, Mater. High Temp. 29 (2012) 145–150.

[10] F.A. Khalid, S.E. Benjamin, The effect of deformation substructure on the high-temperature oxidation of Inconel 625, Oxid. Met. 54 (2000) 63–71.

[11] D. Kim, C. Jang, W. Ryu, Oxidation characteristics and oxide layer evolution of Alloy 617 and Haynes 230 at 900°C and 1100°C, Oxid. Met. 71 (2009) 271–293.

[12] G.A. Greene, C.C. Finfrock, Oxidation of Inconel 718 in air at high temperatures, Oxid. Met. 55 (2001) 505–521.

[13] B.R. Barnard, P.K. Liaw, R.A. Buchanan, D.L. Klarstrom, Effects of applied stresses on the isothermal and cyclic high-temperature oxidation behaviour of superalloys, Mater. Sci. Eng. A 527 (2010) 3813–3821.

[14] P.J. Ennis, W.J. Quadakkers, Corrosion and creep of nickel-base alloys in steam reforming gas, in: J.B. Marriot, M. Merz, J, Nikoul, J. Ward (Eds.), High temperature alloys – Their exploitable potential, Elsevier London, 1988, pp.465–474.

[15] G.C. Wood, T. Hodgkiess, D.P. Whittle, A comparison of the scaling behaviour of pure iron-chromium and nickel–chromium alloys in oxygen, Corr. Sci. 6 (1966) 129–147

[16] H. Ackermann, G. Teneva-Kosseva, K. Lucka, H. Koehne, S. Richter, J. Mayer, Oxidation behaviour of selected wrought Ni-base high temperature alloys when used as flame tube material in modern blue flame oil burners, Corr. Sci.49 (2007) 3866–3879.

[17] H. Buscail, S. Perrier, C. Josse, Oxidation mechanism of the Inconel 601 alloy at high temperatures, Mater. Corros. 62 (2011) 416–422.

[18] S. Cruchley, H.E. Evans, M.P. Taylor, M.C. Hardy, S. Stekovic, Chromia layer growth on a Ni-based superalloy: Sub-parabolic kinetics and the role of titanium, Corros. Sci. 75, (2013) 58-66.

[19] S. Cruchley, M.P. Taylor, R. Ding, H.E. Evans, D.J. Child, M.C. Hardy, Comparison of chromia growth kinetics in a Ni-based superalloy, with and without shot-peening, Corros. Sci. 100 (2015) 242-252.

[20] H.E. Evans, D.A. Hilton, R.A, Holm, S.J. Webster, The influence of a titanium nitride dispersion in the oxidation behaviour of 20%Cr-25%Ni stainless steel, Oxid. Met. 55 (1978) 473-485.

[21] D. Caplan, A. Harvey, M. Cohen, Oxidation of chromium at 890°-1200°C, Corros. Sci. 3, 161 (1963) 161-175.

[22] D. Caplan, G.I. Sproule, Effect of oxide grain structure on the high-temperature oxidation of Cr, Oxid. Met. 9, 459 (1975) 459-472.

[23] E.A. Gulbransen, K.F. Andrew, Kinetics of oxidation of chromium, J. Electrochem. Soc. 104, 334 (1957).334-338.

[24] A. Holt, P. Kofstad, Electrical conductivity of Cr_2O_3 doped with TiO_2, Sol. State Ionics 117 (1999) 21–25.

[25] A. Atkinson, M.R. Levy, S. Roche, R.A. Rudkin, Defect properties of Ti-doped Cr_2O_3, Sol. State Ionics 177 (2006), 1767–1770.

[26] H. Nagai, M. Okabayashi, Ti in Ni20Cr, Deleterious effect of Ti addition on the oxidation resistance of Ni-20Cr Alloy, Trans of the Japan Institute of Metals, 22, (1981), 691-698.

[27] S. Pedrazzini, B.S. Rowlands, A. Turk, I.M.D. Parr, M.C. Hardy, P.A.J. Bagot, M.P. Moody, E. Galindo-Nava, and H.J. Stone, Partitioning of Ti and Kinetic Growth Predictions on the Thermally Grown Chromia Scale of a Polycrystalline Nickel-Based Superalloy, Metallurgical and Materials Transactions A, 50A, (2019) 3024-3029.

[28] H.S. Kitaguchi, I.P. Jones, Y.L Chiu, R. Ding, M.C. Hardy, P. Bowen, Mesoscopic quantitative chemical analyses using STEM-EDX in current and next generatin polycrystalline Ni-based superalloys, Ultamicroscopy, 204, (2019) 55-72.

[29] A. Jalowicka, W. Nowak, D. Naumenko, L. Singheiser, W.J. Quadakkers, Effect of nickel base superalloy composition on oxidation resistance in SO2 containing, high pO_2 environments, Materials and Corrosion, 65, (2014), 178-187.

[30] K. Wollgarten, T. Galiullin, W.J. Nowak, W.J. Quadakkers, D. Naunemko, Effect of alloying additions and presence of water vapour on short-term air oxidation behaviour of cast Ni-base superalloys, Corrosion Science, 173 (2020), 108774, 1-11

[31] A. Jalowicka, W. Nowak, D.J. Young, V. Nischwitz, D. Naumenko, W.J. Quadakkers, Boron depletion in a nickel base superalloy induced by high temperature oxidation, Oxid. Met. 83, (2015), 393-413.

[32 ~~28~~] H.J.T. Ellingham, Reducibility of oxides and sulphides in metallurgical processes, J. Soc. Chem. Ind (London), 63 (5): 125, doi:10.1002/jctb.5000630501.

[33 ~~29~~] D-G He, Y.C. Lin, L-H Wang, Q. Wu, Z-H. Zu, H. Cheng, Influences of pre-precipitated δ phase on microstructures and hot compressive deformation features of a nickel-based superalloy, Vacuum, 161, (2019), 242-250.

[34 ~~30~~] K. Arnold, G. Tatlock, C. Kenel, A. Colella, P. Matteazzi, High temperature isothermal oxidation behaviour of an oxide dispersion strengthened derivative of IN625, Materials at High Temperatures, (2018) 35, 141–150 https://doi.org/10.1080/09603409.2017.1393145

[35 ~~31~~] S. Pedrazzini, D.J. Child, G. West, S.S. Doak, M.C. Hardy, M.P. Moody, P.A.J. Bagot, Oxidation behaviour of a next generation polycrystalline Mn containing Ni-based superalloy, Scripta Materialia, 113 (2016) 51-54.

[36 ~~32~~] L. Garcia-Fresnillo, A. Chyrkin, C. Boehme, J. Barnikel, F. Schmitz, W. J. Quadakkers, Oxidation behaviour and microstructural stability of alloy 625 during long-term exposure in steam, J Mater Sci (2014) 49:6127–6142. DOI 10.1007/s10853-014-8344-7

[37 ~~33~~] A. Chyrkin, P. Huczkowski, V. Shemet, L. Singheiser, W. J. Quadakker. Sub-Scale depletion and enrichment processes during high temperature oxidation of the nickel base alloy 625 in the temperature range 900–1000 ºC Oxidation of Metals (2011) 75:143–166

[38 ~~34~~] Hardy M, Reed R, Crudden D, (2018), European Patent Specification EP 3 112 485 B1, 15 August 2018.

[39 ~~35~~] Hardy MC, Reed RC, Crudden D, (2019), United States Patent US 10,266,919 B2, 23 April 2019.

[40 ~~36~~] Hardy MC, Reed RC, Crudden D, (2019), United States Patent US 10,422,024 B2, 24 September 2019.

[41 ~~37~~] Craven A.J., He K., Garvie L.A., Baker T.N., Complex heterogeneous precipitation in titanium-niobium microalloyed Al-killed HSLA steels-I. (Ti,Nb)(C,N) particles, Acta mater. 48 (2000) 3857-3868.

[42 ~~38~~] Jia Z., Misra R.D.K., O'Malley R., Jansto S.J., Fine-scale precipitation and mechanical properties of thin slab processed titanium-niobuim bearing high strength steels, Materials Science and Engineering A 528 (2011) 7077-7083.
[43 ~~39~~] Jung J-G., Park J-S., Kim J., Lee Y-K., Carbide precipitation kinetics in austenite of a Nb-Ti-V microalloyed steel, Materials Science and Engineering A 528 (2011) 5529-5535.

TABLES

Table 1

Nominal composition of development alloy [38-40].

wt.%	Ni	Cr	Co	Mo	Nb	Ti	Ta	Al	W	Zr	C	B	Fe	Mn	Si	Hf
min	bal	11.5	14.6	2.00	1.20	2.60	3.50	2.90	3.30	0.05	0.02	0.010	0.8	0.20	0.10	0.000
max	bal	13.0	15.9	2.40	1.80	3.10	5.10	3.30	3.70	0.11	0.06	0.030	1.2	0.60	0.60	0.045

Table 2

Values of n, k_n and k_p for the mass change data obtained from the 100 hour thermal cycle tests for the polished variant of the alloy at temperatures shown.

Temp / ºC	n	k_n / (mg cm^{-2})^n.s^{-1}		n	k_p / mg^{2}cm^{-4}s^{-1}
700	2.06	1.513 x 10^{-9}		2	1.513 x 10^{-9}
750	2.2	7.127 x 10^{-9}		2	9.66 x 10^{-9}
800	2.4	41.6 x 10^{-9}		2	33.3 x 10^{-9}

Table 3

Values of k_p determined for the polished and shot-peened surface variants of the alloy under isothermal oxidation conditions at temperature shown.

Temp / °C	Polished	Shot-peened
	k_p / mg^2 cm^{-4} s^{-1}	k_p / mg^2 cm^{-4} s^{-1}
700	0.66 x 10^{-9}	0.58 x 10^{-9}
750	11.0 x 10^{-9}	11.0 x 10^{-9}
800	48.0 x 10^{-9}	39.0 x 10^{-9}
850	550 x 10^{-9}	1700 x 10^{-9}

Table 4

Mass change / surface area (Δm/SA) of polished variant of alloy following 150 hours exposure at the temperatures shown.

Temp / °C	800ºC	810ºC	820ºC	830ºC	840ºC	850ºC
Δm/SA /mg cm^{-2}	0.1610	0.2182	0.1630	0.2610	0.2970	0.3330
k_p / mg^2 cm^{-4} s^{-1}	48.0 x 10^{-9}	88.2 x 10^{-9}	49.2 x 10^{-9}	126.2 x 10^{-9}	163.3 x 10^{-9}	205.4 x 10^{-9}

FIGURES

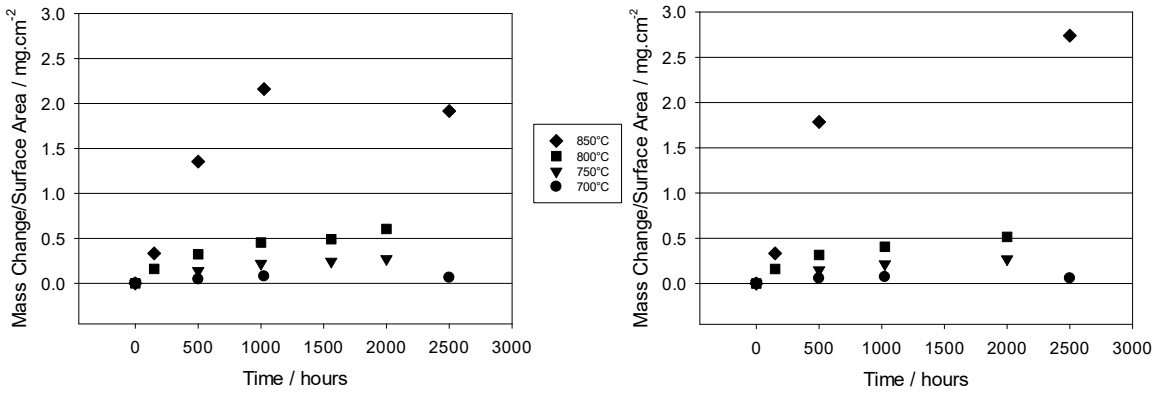

(a) (b)

Fig. 1. Plots of mass change / surface area against time in hours for each temperature under isothermal oxidation conditions showing the similarity in the values obtained for the (a) polished and (b) shot-peened surfaces. The data obtained at 850 °C departed from the trend observed in the oxidation kinetics at the lower temperatures and demonstrated greater sample-to-sample variation.

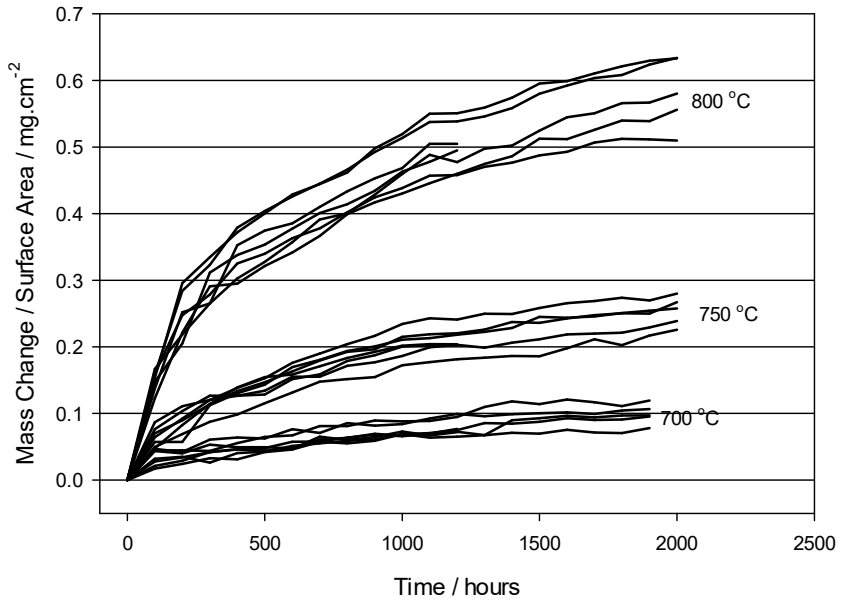

Fig. 2. Plots of mass change / surface area against time in hours for each polished sample exposed under 100 hour thermal cycling conditions showing the range of data collected at each temperature and the influence of temperature on the oxidation process.

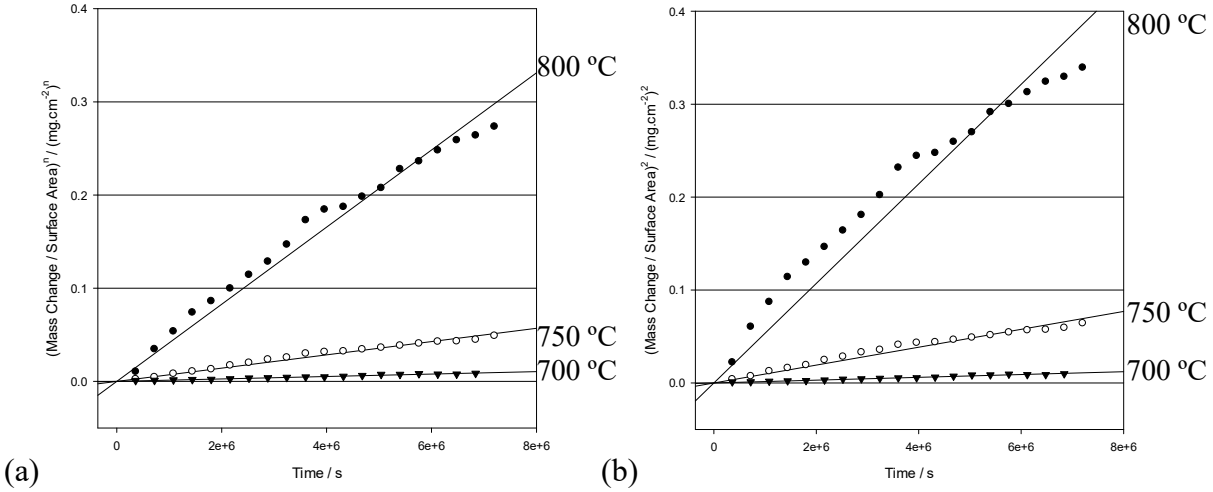

~~**Fig. 3.** Plots of the 100 hour thermal cycled data as (a) (mass change / surface area)^n against time in seconds, using the values of *n* presented in Table 2, and (b) (mass change / surface area)^2 against time in seconds, for each temperature. The gradients of these plots provided the rate constants, k_n and k_p, (a) and (b), respectively. Values are given in Table 3. As can be seen the data fits well to parabolic behaviour especially at the lower temperatures.~~

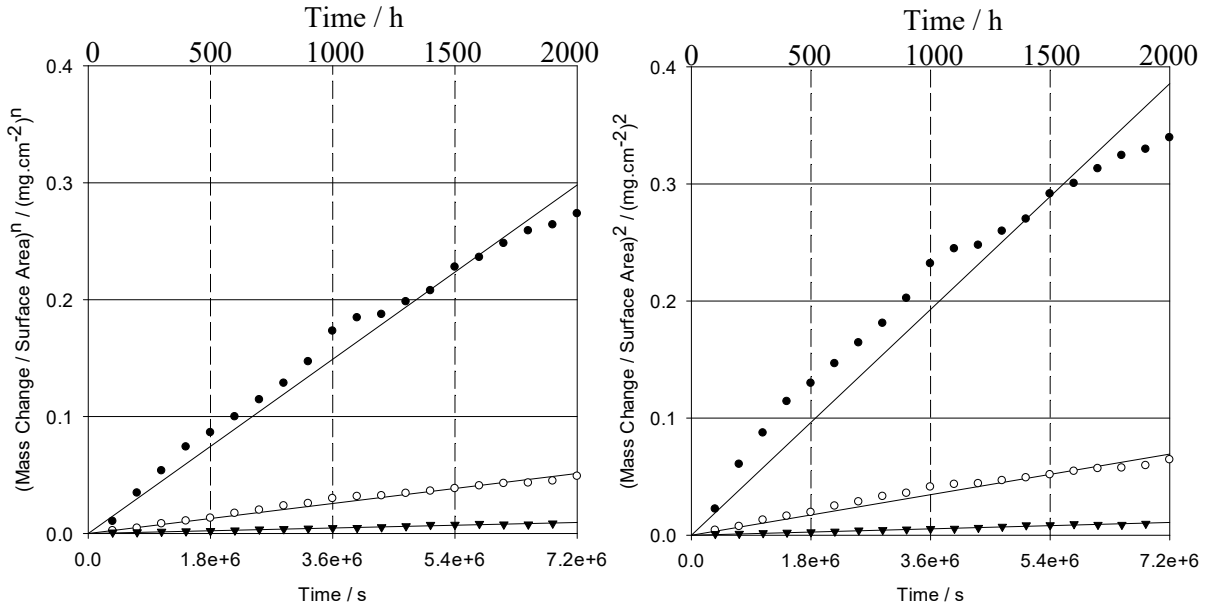

Fig. 3. Plots of the 100 hour thermal cycled data as (a) (mass change / surface area)^n against time in seconds, using the values of *n* presented in Table 2, and (b) (mass change / surface area)^2 against time in seconds, for each temperature. The time in hours is also shown. The gradients of these plots provided the rate constants, k_n and k_p, (a) and (b), respectively. Values are given in Table 3. As can be seen the data fits well to parabolic behaviour especially at the lower temperatures.

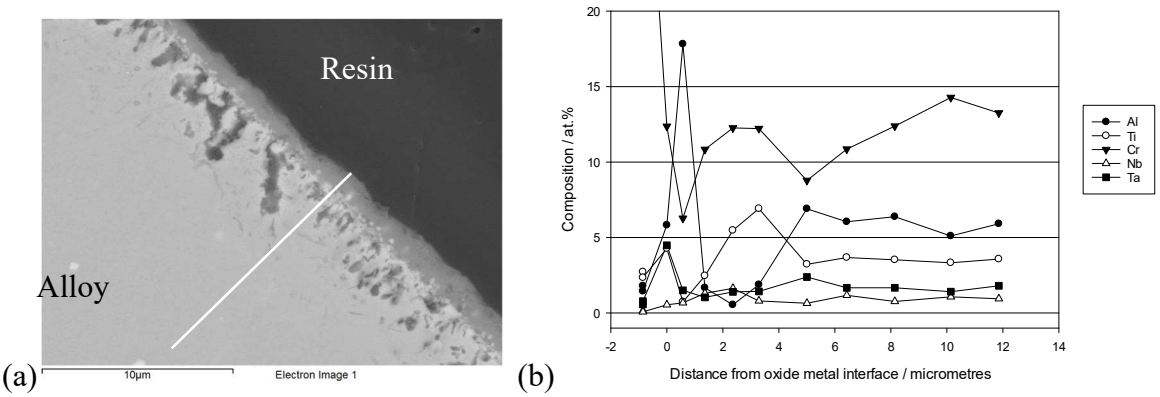

Fig. 4. (a) SEM image in back scatter mode of a cross-section through a sample of the polished variant of the alloy exposed at 800 °C for 2000 hours under isothermal conditions showing the formation of a surface layer of oxide with internal dark contrast changes to the alloy in the sub-surface region, and (b) EDS elemental profiles of alloying elements from site indicated by solid line in (a), with the interface between the oxide and the alloy set as zero, showing depletion of aluminium but an enhancement of titanium in the sub-surface region of the alloy.

.

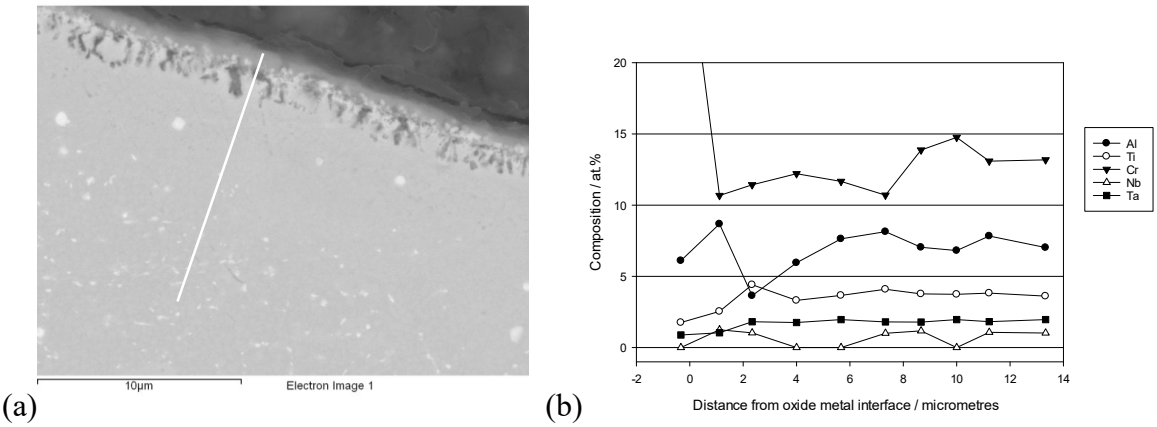

Fig. 5. (a) SEM image in back scattered mode of a cross-section through a sample with a shot-peened surface finish exposed at 800 °C for 1025 hours under isothermal conditions, and (b) EDS elemental profiles, with the interface between the oxide and the alloy set as zero, showing a chromium-rich surface oxide with depletion of aluminium but little change in the profiles of the other minor elements present in the sub-surface region of the alloy.

(a)

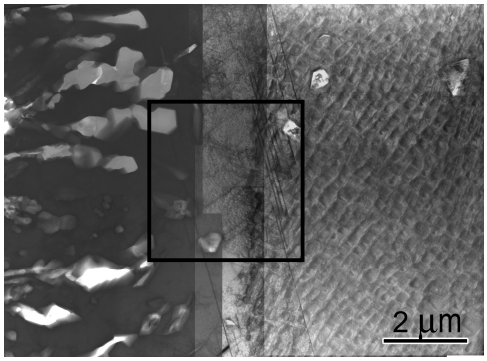

(b)

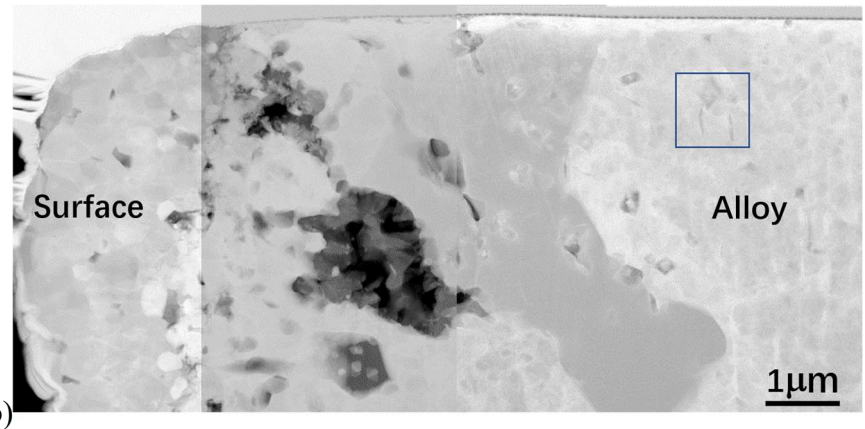

Fig. 6. Montage of STEM images of: (a) a polished variant of the alloy exposed to 800 ºC for 2000 hours showing, from left to right, ~~recrystallised~~ modification to the microstructure due to elemental depletion of the alloy beneath the surface oxide (not shown), internal Al_2O_3 in light contrast, a planar interface between the oxidation affected region and the unaffected alloy, and (b) a shot-peened variant exposed to 800 °C for 1025 hours showing, from left to right, the surface oxide, internal Al_2O_3, recrystallisation of the alloy grains adjacent to the surface oxide and an undulating interface with the unaffected alloy. Also shown are precipitates indicted by arrows. Boxes indicate the sites from which higher magnification and EDS maps were taken (Figs.7 and 8).

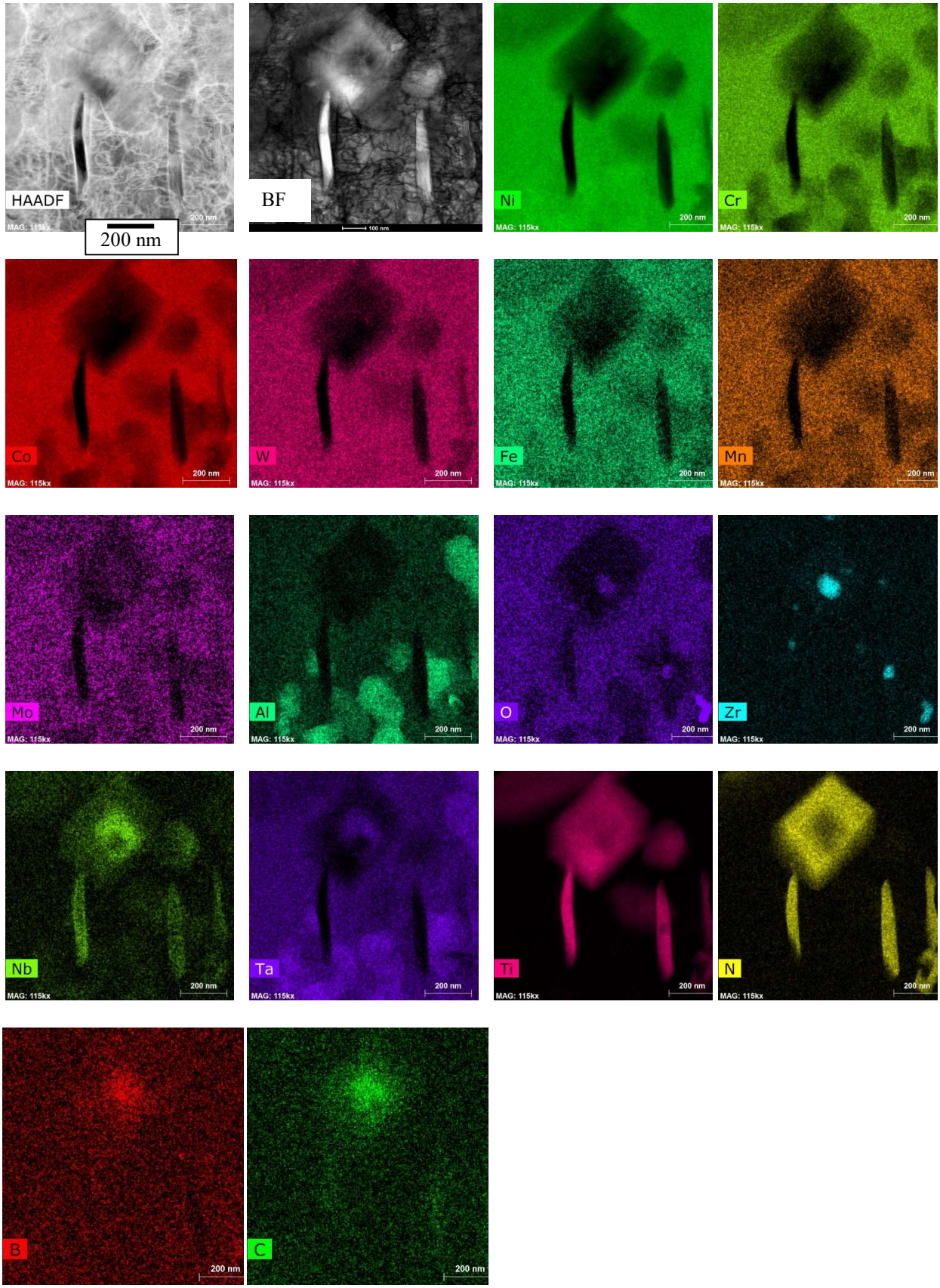
HAADF
200 nm
BF
Ni
Cr
Co
W
Fe
Mn
Mo
Al
O
Zr
Nb
Ta
Ti
N
B
C

Fig. 7. TEM images with EDS maps taken from the sample with a shot-peened surface finish exposed under isothermal conditions for 1025 hours at 800ºC showing compositional and morphology details of two types of precipitates distributed throughout the alloy: a cubic shaped phase with a zirconium oxide centre surrounded by layers of Nb, Ta and Ti and a high aspect ratio phase of Nb and Ti aligned along dislocations pile-ups, higher nitrogen, carbon and boron signal compared to the matrix show these to be a mixture of nitrides, carbides and borides.

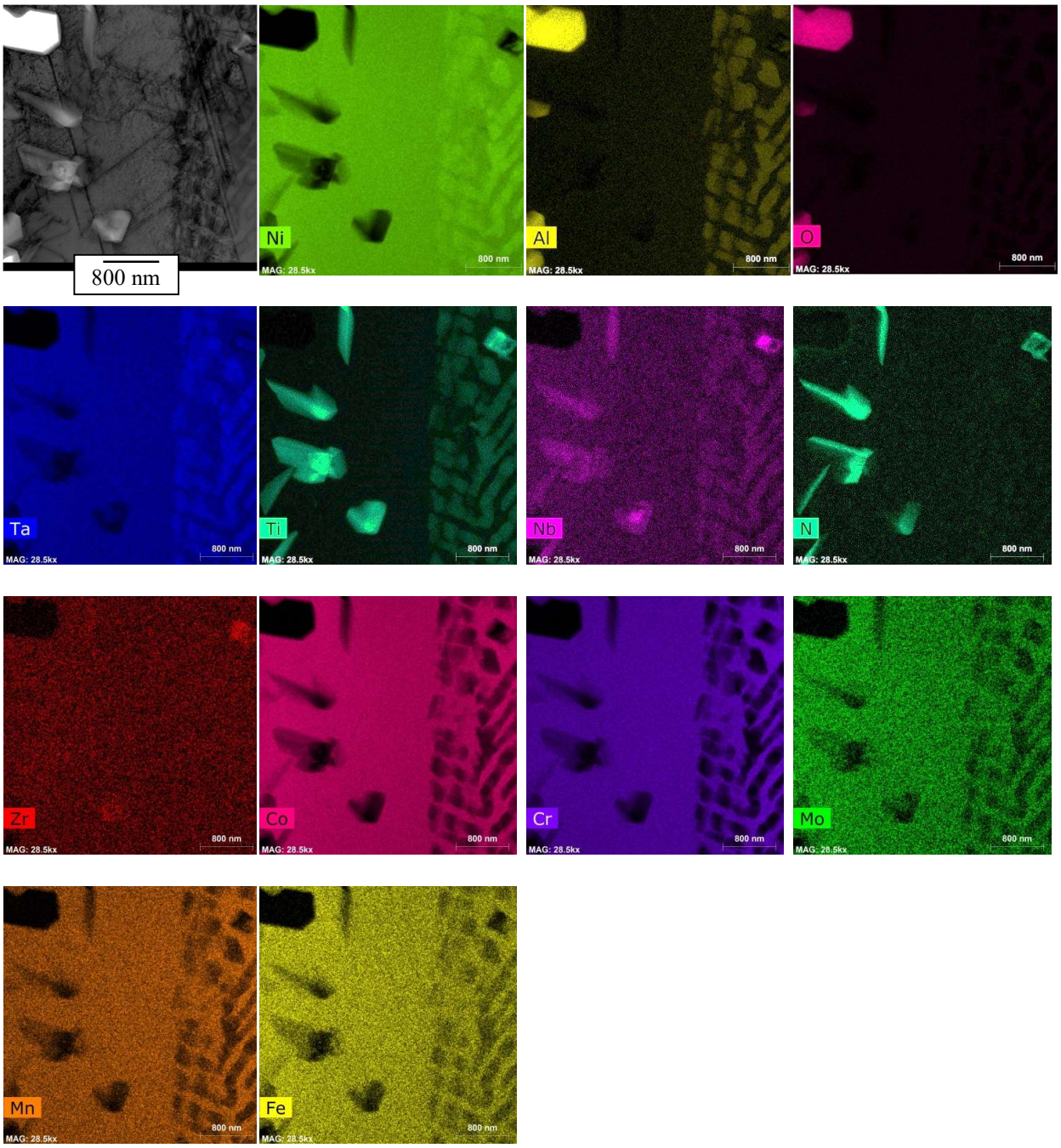

Fig. 8. TEM image with EDS maps taken from the sample with a polished surface exposed under isothermal conditions for 2000 hours at 800ºC showing the distribution of the elements in the sub-surface region of the alloy resulting from changes occurring due to the oxidation process (left-hand side of images) and including phases present in the unaffected alloy (right-hand side).

This Figure has been modified to reduce number of maps to reduce the size of the figure while still emphasising the changes occurring to the precipitates within the oxidation affected zone.

See modified Fig. 8 below.

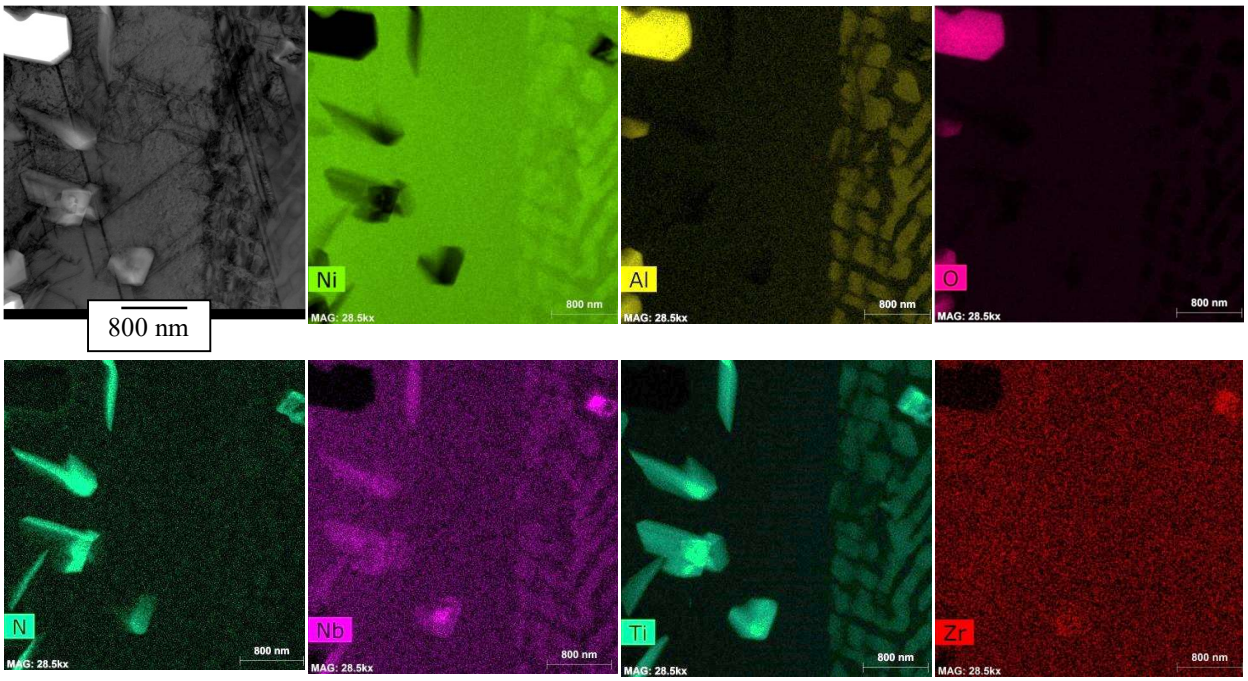

Fig. 8. TEM image with selected EDS maps taken from the sample with a polished surface exposed under isothermal conditions for 2000 hours at 800ºC showing the interface between the unaffected γ/γ′ region (right-hand side) and the oxidation affected region (left-hand side of images). The distribution of the elements demonstrates that the nitrogen containing precipitates in the oxidation affected region have grown.

Modified Figure

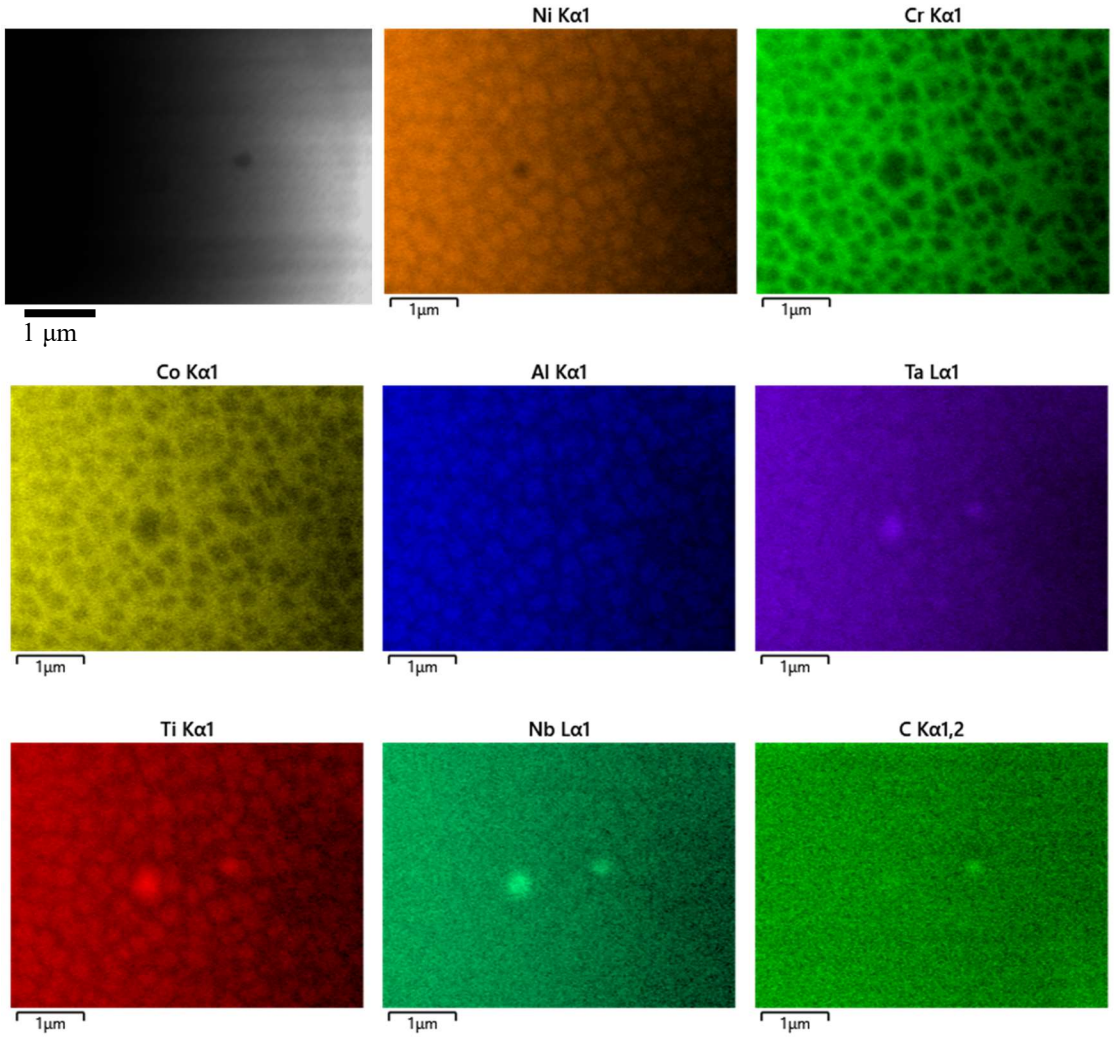

Fig. 9. Transmission image of foil taken from the as-received alloy with selected EDS maps showing the distribution of elements in the matrix associated with the γ / γ′ structure and the presence of titanium, tantalum and niobium associated with the carbon.

New Figure

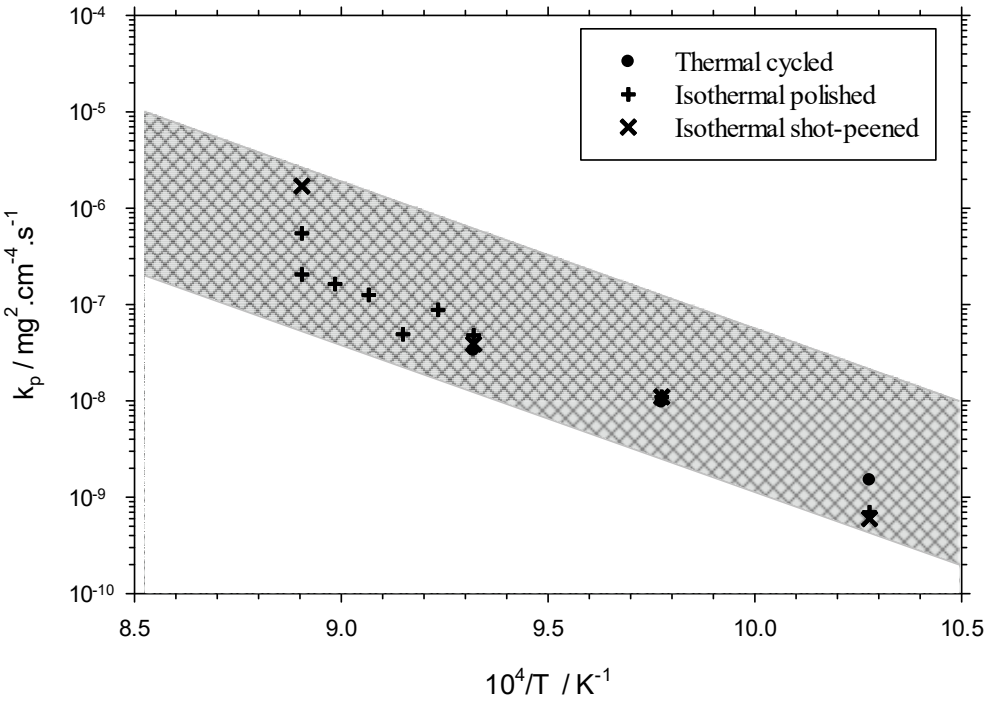

Fig. 10. Arrhenius plot of *ln kp* against the inverse of the temperature in K for all samples, see legend for testing details. The hashed region shows the range of data for comparable alloys [5-19] with the lower boundary corresponding the formation of pure Cr_2O_3 [20-23]. The data up to 840 °C lies towards the lower bound and the gradient gave a value of 269 kJ mol^{-1} for the activation energy for the oxidation process for the development alloy. Over 840 840 °C the kinetics move towards the upper boundary.